Technical Article

- Development of Indigenous SEESPEC Code for the Modeling and Simulation of Solvent Extraction Process

Young Researcher's FORUM

- Post Synthetic Modification of Metal-Organic Frameworks for Development of Phosphors and Sensing / Recovery of U(VI)

News and Events

- Azadi ka Amrit Mahotsav Indira Gandhi Centre for Atomic Research Program on Anu Awareness – a brief report
- DAE-ICONIC Week Celebration Indira Gandhi Centre for Atomic Research

Awards, Honours and Recognitions

Bio-diversity @ DAE Campus, Kalpakkam

Director's Message

Dear Readers,

It gives me immense pleasure to share with you the series of programs conducted by IGCAR as part of "Azadi ka Amrit Mahotsav" to commemorate the 75th Independence Day. Nuclear Science Yatra was carried out to create awareness on nuclear science and technology and highlight the activities of the Department of Atomic Energy among the youth, especially in the rural areas of all districts in Tamil Nadu. The yatra started at Kalpakkam and culminated at Kudankulam, covering a distance of more than 1000 km. It was flagged off by Chief Administrative Officer and it covered 10 institutions. Each of these institutions served as a nodal point where exhibitions and competitions were conducted and more than 2000 students participated in the exhibitions. IGCAR and GSO, had organized a sand art sculpture in the Kalpakkam beach during August 27-28, 2022 depicting various technologies of DAE applied to the societal benefits. The sculpture was inaugurated by Revenue Divisional Officer, Chengalpattu Smt. Shajeevana IAS. IGCAR also organized a one day awareness event in the higher secondary school, Sadurangapattinam as a part of DAE-ICONIC week. As a part of the event, mathematician Shri Jothi Lingam, Retired Station Master, Indian Railways explained generation of magic square to the students.

Important achievements of various groups of IGCAR were highlighted during the 75th Independence Day. FBTR has operated for 78 effective full-power days generating about 15.6 million units of electricity. UO_2 pin chopping was inaugurated at DFRP. The incubation centre has transferred four technologies to various companies. I appreciate the efforts of the editorial committee and the author's contributions to the Newsletter.

Jai Hind

(B. Venkatraman)

Director, IGCAR

Editor's Desk

Dear Reader
Greetings

It is my pleasant privilege to forward the latest issue of IGC Newsletter (Volume 134, October 2022, Issue 4). I thank my team for their timely inputs, cooperation, and support in bringing out this issue.

The digital copy is published at http://www.igcar.gov.in and is available on the intranet at http://vaigai as a flip copy.

Director's message is a discussion on the series of programs conducted by IGCAR as a part of "Azadi ka Amrit Mahotsav" to commemorate the 75th Independence Day.

In this issue, One technical article "Development of Indigenous SEESPEC Code for the Modeling and Simulation of Solvent Extraction Process" by Dr. S. Balasubramonian and his colleague from RRDD, Reprocessing Group, IGCAR.

Young Officer's Forum features an article on "Understanding the formation mechanism of SFT in FCC metals: An atomistic simulation study" by Shri Arun Kumar Panda from PMD, MCG, IGCAR.

The young researcher is Mrs. Vaddanam Venkata Sravani is working towards her doctoral degree from HBNI at the solution chemistry and mass spectrometry studies Section, MC&MFCG, IGCAR. Her article is on "Post Synthetic Modification of Metal-Organic Frameworks for Development of Phosphors and Sensing / Recovery of U(VI)".

I am happy to share the awards and honors earned by our colleagues from July to October 2022.

In this issue, back cover is adorned by Ashy Prinia which is found throughout the year in Kalpakkam.

The Editorial Committee would like to thank all the contributors. We look forward to receiving constructive suggestions from readers towards improving the IGC Newsletter content.

We express our deepest gratitude to Director IGCAR for his keen interest and guidance.

With best wishes and regards

S. Rajeswari

Chairman, Editorial Committee, IGC Newsletter and

Head, Scientific Information Resource Division, IGCAR

Development of Indigenous SEESPEC Code for the Modeling and Simulation of Solvent Extraction Process

The spent nuclear fuel is reprocessed for the recovery of uranium and plutonium by a liquid-liquid extraction procedure, known as the PUREX process. The spent nuclear fuel dissolver solution is composed of U(VI), Pu(IV), fission products and corrosion products in 3 - 5 M nitric acid medium. The fissile and fertile elements such as uranium and plutonium present in the dissolver solution are extracted into the organic solvent phase composed of 1.1M tri-n-butyl phosphate (TBP) in n-dodecane (n-DD). The driving force for the extraction of U(VI) and Pu(IV) in organic phase is due to the differences in the chemical potential of these elements in organic and aqueous phases. The mass transfer occurs until the chemical potential of these elements in both the phases becomes equal and at this point the liquid-liquid extraction is said to have attained the state of equilibrium. The distribution coefficient is one of the important parameters invoked in liquid-liquid extractions to understand degree of mass transfer, solvent requirement, and thermodynamic stability of the extracted species in organic phase. The distribution coefficient is defined as the ratio of the concentration of solute in organic to aqueous phase at equilibrium.

In liquid-liquid extractions, the aqueous phase is contacted multiple times with organic phase at the required organic to aqueous phase volume ratio to quantitatively extract the solute in to organic phase. Now a days, the optimization of such multi-stage extraction process, known as the solvent extraction flow-sheet, as well as the process design of multi-stage solvent extraction is often carried out with the help of computer simulation. The conventional procedure based on Mccabe Thiele diagram for optimizing the flow-sheet is unsuitable for such purpose owing to the multi-component nature of the feed solution and also to the interdependence of distribution coefficients in a multi-component system.

The computer code envisaged for the simulation of solvent extraction flow-sheet consists of two parts. The first part of the code comprises of a model for estimating the distribution coefficient of metal ions and the second part of the code solves the multi-stage mass balance equation. Development of an accurate model for estimating the distribution coefficient is one of the prerequisites for the reliable simulation of solvent extraction flow-sheet. Several models have been reported in literature for estimating the distribution coefficient of metals of commercial and strategic important. However due to its commercial value confidentiality, complete knowledge of these models is not available in open literature except few codes, for instance the SEPHIS code for strategic materials. This code is

essentially developed for the extraction of U(VI) and Pu(IV) from the dissolver solution arising from spent thermal reactor fuels, wherein the concentration of U(VI) is significantly higher (>98%) than Pu(IV). However the accuracy of SEPHIS code for the estimation of distribution coefficient from the aqueous solution having higher concentration of Pu(IV) is quite less. In view of this, the SEPHIS code is not suitable for the simulation of solvent extraction flow-sheet in fast reactor fuel reprocessing. Therefore, there is a need to develop advanced computer codes based on thermodynamic approach for profiling the plutonium and uranium in process streams arising from fast reactor fuels. In this context, an indigenous code namely "Solvent Extraction Equilibrium Speciation Calculation" (SEESPEC) has been developed at Reprocessing Group, IGCAR and evaluated for fast reactor fuel reprocessing application, as discussed below.

Thermodynamic model for the estimation of distribution coefficient

In this theoretical approach, the extraction of U(VI) and Pu(IV) in the organic phase is considered as a complex formation reaction, shown in Eq. (1). The species in the organic phase are denoted as over bar.

$$M^{n+} + n\,NO_3^- + z\,\overline{TBP} \leftrightarrow \overline{M(NO_3)_n \cdot zTBP} \qquad (1)$$

Thermodynamic equilibrium constant (K) for the above reaction based on the law of mass action is shown in equation 2.

$$K = \frac{a_{\overline{M(NO_3)_n \cdot zTBP}}}{a_{M^{n+}}\, a_{NO_3^-}^n\, a_{\overline{TBP_f}}^z} \qquad (2)$$

According to the law of mass action principle, the thermodynamic equilibrium constant is the quotient of product of activity of product to the activity of the reactant. By rearranging the above equilibrium relation, the distribution coefficient of metal ion (K_d) can be expressed as follows

$$K_d = K\,[NO_3^-]^n\, \overline{[TBP_f]}^z\, \frac{\gamma_{NO_3^-}^n\, \gamma_{M^{n+}}\, \gamma_{\overline{TBP_f}}^z}{\gamma_{\overline{M(NO_3)_n \cdot zTBP}}} \qquad (3)$$

Where $[NO_3^-]$ and $[TBP_f]$ are the concentration of nitrate ion and free TBP respectively. γ is the activity coefficient of species. It is noted that the distribution coefficient is the function of nitrate ion concentration, free TBP concentration and the ratio of activity coefficient of species. The unknown parameter in Eq. (3) is the equilibrium constant and activity coefficients. Determination of activity coefficient of the species involved in Eq. (3) is very complex and in the present study, it was determined by electrolyte
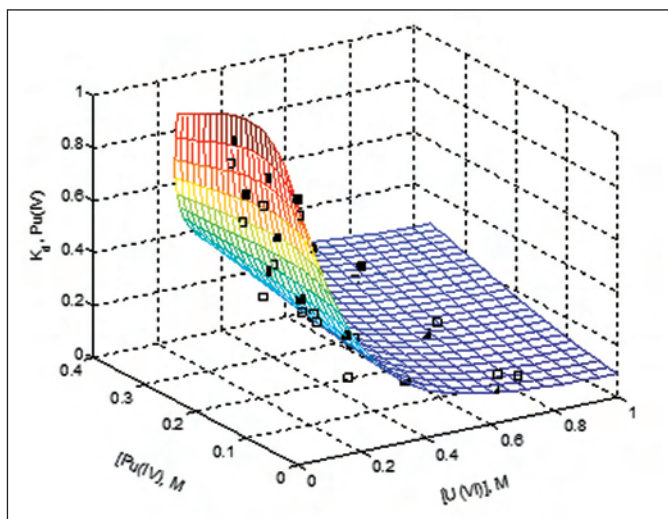
Fig 1: Variation in the distribution coefficient of Pu(IV) as a function of U(VI) and Pu(IV) concentration at a fixed HNO$_3$ concentration of 0.5 M (☐ Literature data, ▌Calculated by SEESPEC)

Fig 2: The absolute percentage error for the estimation of distribution coefficient of Pu(IV) using SEESPEC and SEPHIS model (○ SEPHIS, ☐ SEESPEC) for various nitric acid concentration (a) 0.5 M HNO$_3$ b) 1M HNO$_3$ c) 3M HNO$_3$ d) 4 M HNO$_3$)

UNIversal QUAsi Chemical (eUNIQUAC) model. The interaction parameters in the activity coefficient model and the the thermodynamic equilibrium constant (K) were estimated from the experimental data. The objective function is formed by the sum of squared deviation between the experimental and estimated distribution coefficient as follows

$$f_{obj\_fn} = \sum_i \left(K_{d,exp,i} - K_{d,pred,i} \right)^2 \qquad (4)$$

The minimization of the above equation is carried out with the optimization routine in MATLAB. In Eq. (3), the activity coefficient of species in the organic phase is assumed as unity, since the interaction of species in the organic phase is simple as compared to the aqueous phase. In view of this, the present approach for modeling of distribution coefficient can be termed as semi-theoretical model owing to the assumption of ideal nature of organic phase.

Solvent extraction flow-sheet simulation

In addition to the development of a model for distribution coefficient, simulation of the solvent extraction flow-sheet requires the complete knowledge on the flow behavior of aqueous and organic phases, agitation speed and non-ideal flow pattern such as axial mixing/back mixing etc. Understanding the flow pattern of the liquids in a solvent extraction contactor is a challenging job and it is often predicted with the application of computational fluid dynamics (CFD) simulation. Another approach to understand the bulk behavior of the solvent extraction contactor is to determine the Murphree stage efficiency. To determine this, several experiments are carried out at various flow rates of aqueous and organic phases and the exit concentration of the solute in these phases are measured. The Murphree stage efficiency is then calculated by comparing the exit and equilibrium concentration of
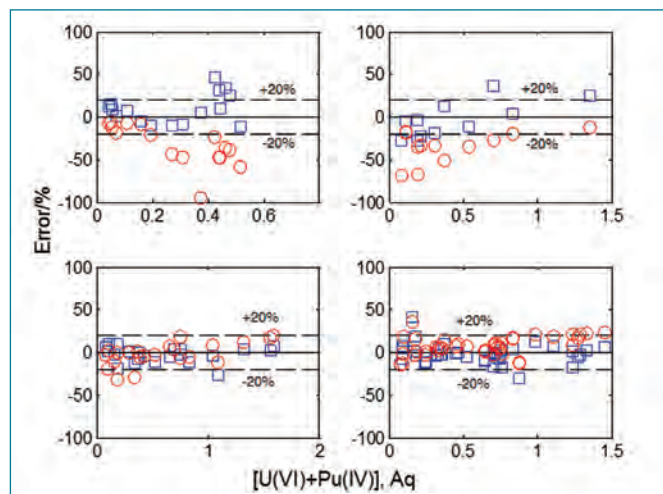
the solute, which can be directly estimated from the distribution coefficient model. The Murphree stage efficiency has been employed in the present study for flow sheet-simulation in the counter current centrifugal extractors. The stage concentration profiles have been estimated by simultaneously solving the time dependent differential mass balance equation combined with the mass transfer of solute from aqueous to organic phase or vice versa.

Development of SEESPEC code

Based on the thermodynamic theoretical background discussed above, an in-house code namely "Solvent Extraction Equilibrium Speciation Calculation" (SEESPEC) has been developed for the estimation of distribution coefficient of U(VI), Pu(IV) and nitric acid in PUREX process condition. The salient feature of the SEESPEC code are the inclusion of the partial dissociation of nitric acid and speciation of Pu(IV) in aqueous nitric acid solution. The formation of various Pu(IV) species in nitric acid solution such as mono-, di-, tetra- and hexa-nitrate species are considered and the relative concentration of Pu(IV) nitrate species as well as the distribution coefficient of Pu(IV) and U(VI) in 1.1M solution of TBP in n-DD as a function of nitric acid concentration were estimated. Figure 1 shows the variation in the distribution coefficient of Pu(IV) estimated from SEESPEC code, plotted as a function of U(VI) and Pu(IV) concentration in 0.5 M nitric acid. The SEESPEC distribution coefficients are compared with the experimental data reported in literature. It can be seen that the distribution coefficient of Pu(IV) increases with the decreasing concentration of U(VI) in aqueous phase, where as the K$_d$ increases with increase in the concentration of Pu(IV). It is important to note that the SEESPEC code precisely follows the experimental data and falls on the mesh in the 3D plot. Similarly, the distribution coefficient of Pu(IV) was
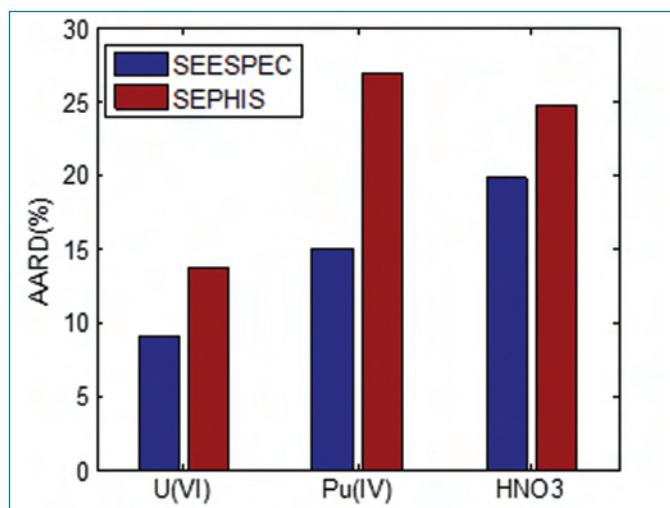
Fig 3: Comparison in the AARD/% of SEESPEC and SEPHIS Codes

estimated from SEESPEC code at all acidities and the variation in the percentage error of the estimated value from the experimental data at various uranium and plutonium concentration are plotted in Figure 2. The data were compared with those obtained using the other code SEEPHIS. The estimated distribution coefficient of Pu(IV) at lower nitric acid concentrations (< 1 M HNO_3) using the SEESPEC model shows lower deviation as compared to the SEPHIS model. The average absolute relative deviation (AARD, %) between the experimental and model estimated distribution coefficient of U(VI), Pu(IV) and HNO_3 is shown in Figure 3. It can be seen that the SEESPEC code gives lower value for AARD (%) as compared to the SEPHIS code. It is noted that the AARD (%) of SEESPEC is nearly half of that determined by SEPHIS especially for the estimation of distribution coefficient of Pu(IV).

Application of the SEESPEC code for DFRP flow sheet simulation

In view of the precise estimation of distribution coefficients and lower AARD%, the SEESPEC code has been employed for the simulation of solvent extraction flow-sheet proposed in the Demonstration Fuel Reprocessing Plant (DFRP) facility. The simulations include the design of solvent extraction flow-sheet, optimization of various parameters in the flow-sheet, estimation of the safe operating envelope of the process for process control applications.

Estimation of Number of Stages for Extraction and Scrubbing

In the first co-decontamination (HA) cycle, the number of stages required for the extraction of uranium & plutonium and scrub stages needed to achieve the required decontamination from fission products was estimated using SEESPEC code. Figure 4a shows the concentration of U(VI) and Pu(IV) in the raffinate as a function of number of stages in the HA cycle. It can be seen that about six extraction stages are required to bring down the concentration of U(VI) and Pu(IV) from 12.35 g/L and 28.8 g/L respectively to 1 mg/L in the aqueous raffinate. Similarly, the Zr(IV) and Ru(III) concentration in the organic product can be brought down to less than 1 mg/L with the employment of nine scrubbing stages.

Operating Envelope for DFRP 1st Stripping Cycle

The stripping of uranium and plutonium is proposed to be carried out in a 22-stage centrifugal extractor bank as shown in Figure 5, in the 1st stripping cycle (HC). Since the radiolytic degradation of organic phase is more during fast reactor fuel reprocessing, due to higher burn-up and plutonium content. Among the various degradation products, the di butyl phosphate (HDBP) forms strong complex with Pu(IV) and U(VI) at lower acidities. As a result, the stripping of actinides especially plutonium from the loaded organic phase in the HC cycle is quite difficult. In order to strip plutonium completely from the loaded organic phase, it is proposed to reduce the strongly complexing Pu(IV) in to weakly complexing Pu(III) using U(IV) as reducing agent and recover the
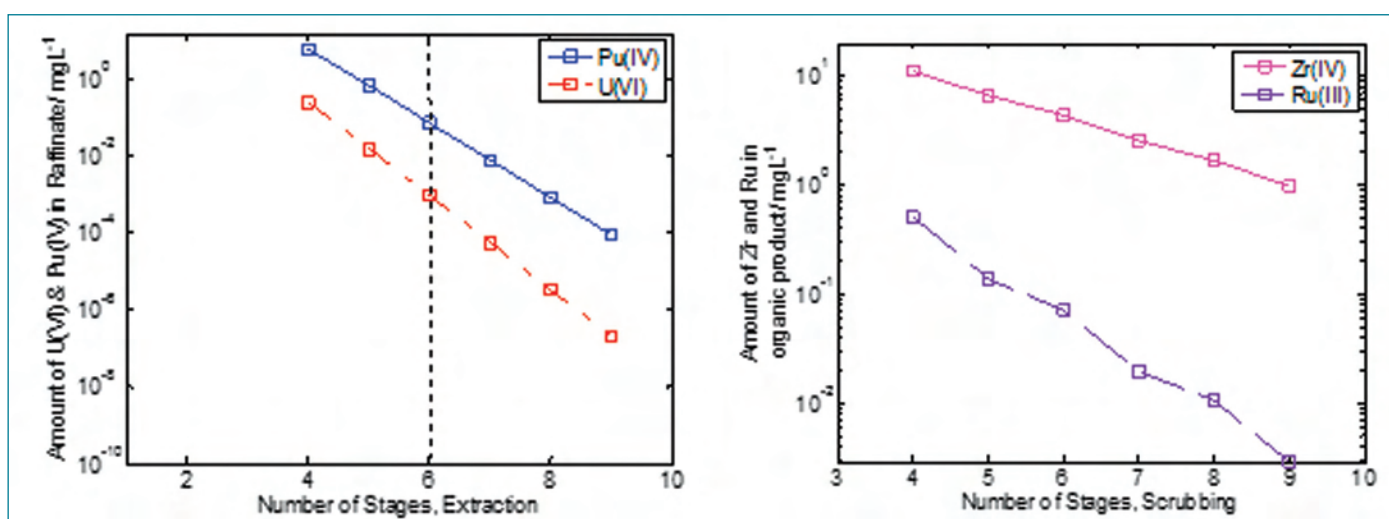
Fig 4: The Concentration of Solutes and Fission Products in Raffinate and Organic Product Stream Estimated by SEESPEC a) U(VI) &Pu(IV) b) Zr(IV) & Ru(II&III)
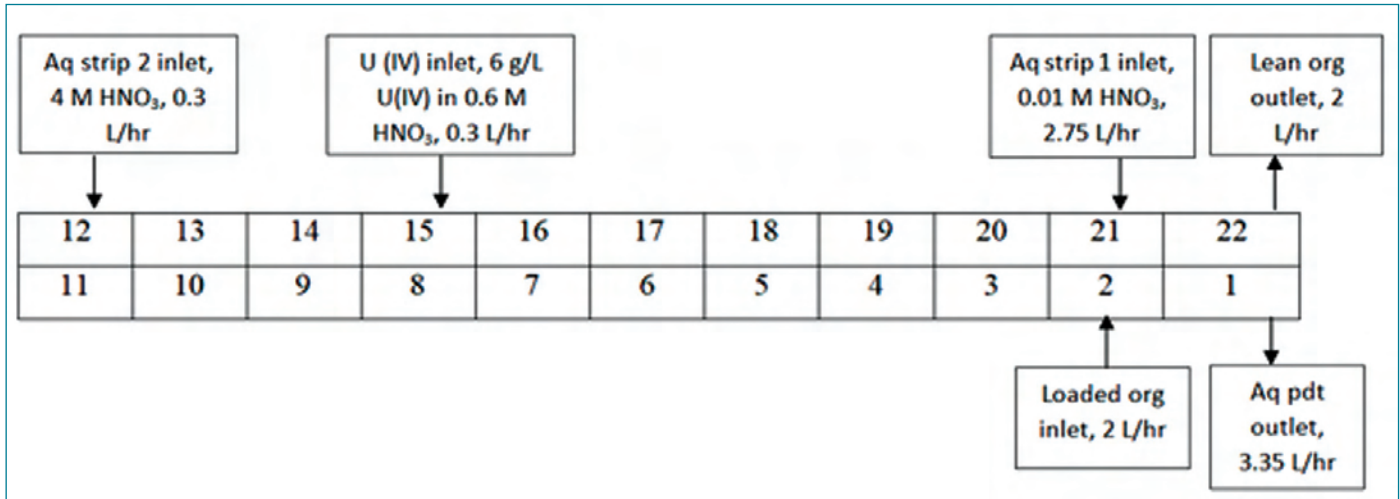
Fig 5: DFRP 1st cycle stripping flow sheet

inextractable Pu(III) from aqueous phase in the HC cycle. However, the location of feeding U(IV) and the flow-rate of U(IV) solution for complete striping of Pu(IV) with minimum consumption of U(IV) is to be determined.

In this context, the optimum feed location for U(IV) and the desired operating envelope for the aqueous strip-1 flow-rate for various loaded organic feed-flow rate was estimated using SEESPEC. The concentration of U(VI) in the lean organic phase as a function of various loaded organic phase flow rate and aqueous strip-1 flow rate is shown in Figure 6. The green color region in the plot indicates the lean organic phase concentration of U(VI) below 1 mg/L, yellow denotes 1-10 mg/L and red denotes more than 10 mg/L. From Figure 6, it is learnt that the flow-rate of organic and aqueous strip-1 can be fixed anywhere in the green region to obtain the lean organic phase concentration below 1 mg/L. However, for the proposed organic flow-rate of 2 L/h in the HC

Fig 6: The Operating Region of Aqueous Strip 1 Flow Rate With 10% More than the Minimum Aqueous Strip 1 Flow Rate For the Organic Feed Flow Rate of 2 L/hr.

bank, a minimum aqueous flow-rate of strip-1 at 2.5 L/h can be fixed to achieve both 1 mg/L uranium in the lean organic phase as well as to minimize the generation of unnecessary aqueous waste. Nevertheless, it is desirous to operate the aqueous strip-1 flow-rate at 2.8 L/h, in order to take care of the 10% variation in flow-rate of aqueous and organic phases under plant operating conditions.

Process Control in DFRP HC Bank

Generally, the radioactive liquids in reprocessing plants are pumped through a low maintenance pumping systems, such as air-lifts. The accuracy of discharge flow during the operation of air lift is quite low as compared to the conventional metering pumps. In the 1st stripping cycle (HC) shown in Figure 5, the air-lift is employed for pumping the loaded organic phase and U(IV) solution. In view of this, it is necessary to understand the effect of variation in the loaded organic phase and U(IV) flow rate on the stripping performance of uranium and plutonium in the HC bank. The dynamic simulation of the HC bank was carried out to study the effect of the flow-rate variation on stripping of actinides. From Figure 5, the proposed set flow rate of the organic phase is 2 L/h and U(IV) flow rate is 0.3 L/h. However these flow rates can decrease or increase depending upon the performance of the air-lift. In the present simulation, the discharge flow-rate of loaded organic phase and U(IV) solution is assumed to be delivered in the form of a pulse shown in Figure 7a and 7b respectively. In the pulse signal, the pulse ON duration represents the elapsed time of change in the flow-rate and OFF signal represents the duration of the set flow-rate. The pulse amplitude represents the magnitude of the variation in the flow rate.
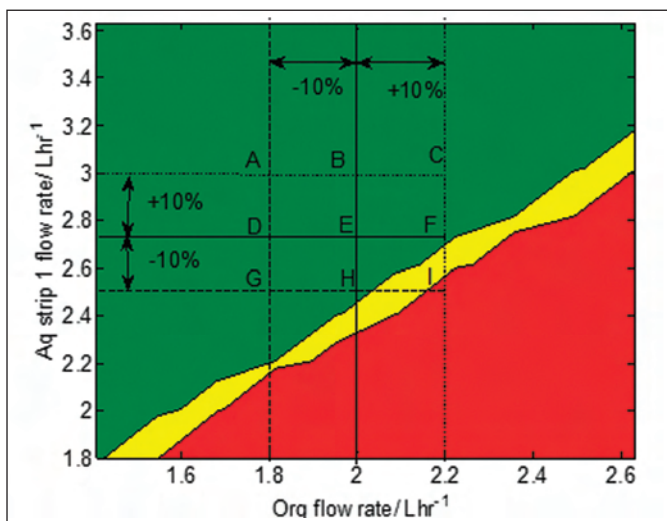
In the present study, the organic flow-rate was varied from 10 to 80 % more than the normal flow rate of 2 L/h i.e from 2.2 (10%) to 3.6 L/h (80%) and U(IV) flow rate is varied from -99 % to 100%, i.e from 0.003 (-99%) to 0.6 L/h (100 %). In Figure 7a
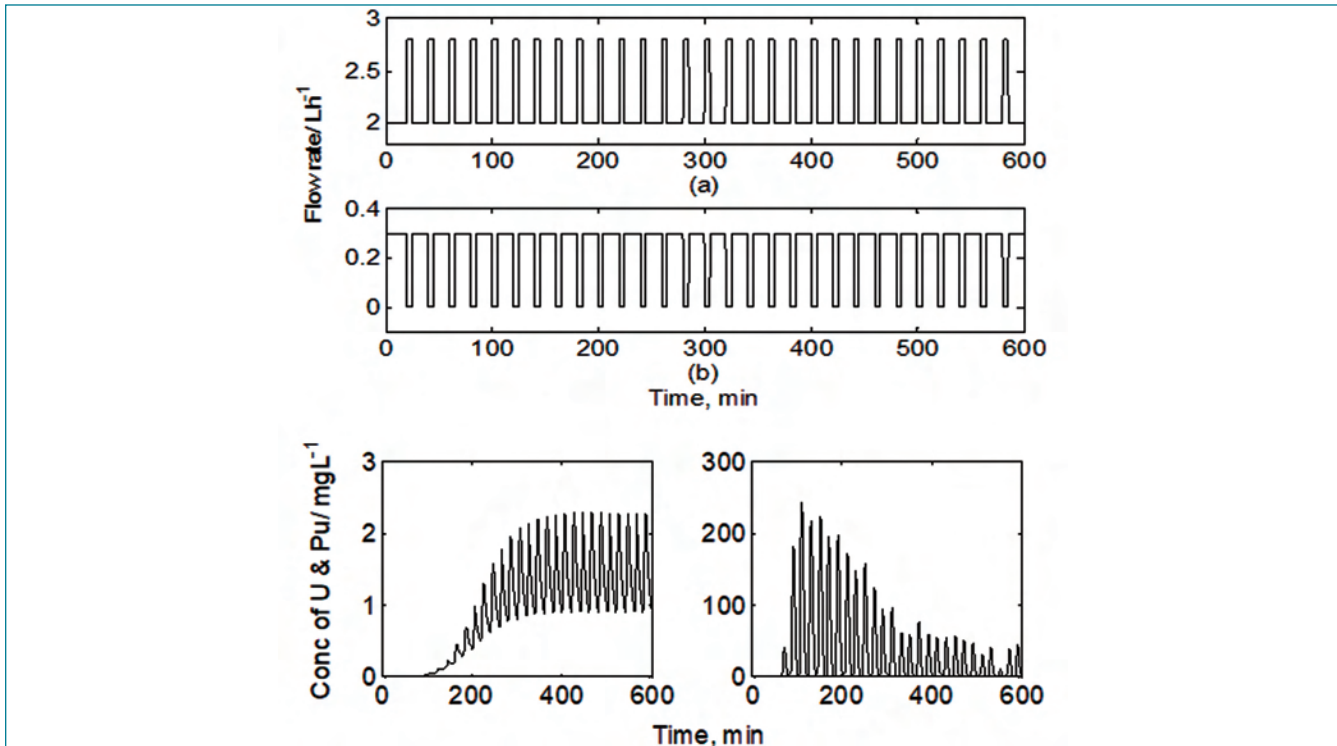
Fig 7: Typical Input Pulse of Organic Feed and U(IV) Stream for 5 min ON Duration with 15 min OFF Interval and the Corresponding Lean Organic Phase Concentration of U and Pu; a) Pulse Input of Organic Feed, b) Pulse Input of U(IV) Flow Rate, c) Org phase Exit Concentration of U/ mgL-1 d) Org phase Exit Concentration of Pu/ mgL-1

and b, the organic flow rate is varied by 40% and U(IV) flow rate is decreased by 99%. The values of other operating parameters such as aqueous strip 1, strip 2 and concentration of HNO3

Fig 8: The exit concentration of U (left side plot) and Pu (right side plot) for various pulse amplitude a) 5 min ON-15 min OFF b) 10 min ON- 15 min OFF c) 15 min ON-15 min OFF d) 20 min ON-15 min OFF (In fig Green zone denotes the concentration below 1 mg/L, Yellow denotes 1-10 mg/L and red denotes more than 10 mg/L)

were fixed at the set value as shown in Figure 5. The SEESPEC dynamic simulation results on the concentration of uranium and plutonium in the lean organic phase outlet for a typical pulse input signal indicated in Figure 7a and b is shown in Figure 7 c & d respectively. It can be seen that the influence of pulse input on the lean organic phase exit is observed only after 100 minute and 50 minute respectively for uranium and plutonium. There after there is a continuous variation in the uranium and plutonium concentration in the lean organic phase exit concentration as shown in Figure 7 c & d.

Figure 8 shows the averaged exit concentration of uranium and plutonium observed at 600 minutes as a function of variation in organic and U(IV) flow rate for various pulse ON duration with fixed OFF duration of 15 min. It is noted that the allowable operating region where the uranium and plutonium concentration in the lean organic phase is less than 1 mg/L (green color region) decreases with the increase of pulse ON duration from 5 minutes (Figure 8a) to 20 minutes (figure 8d). From figure 8, flow rate variation for the safe operation can be predicted easily and accordingly the process can be operated (in the green region) in the plant to minimize the retention of uranium and plutonium in the lean organic phase in HC bank.

Reported by
Dr. S. Balasubramonian and his colleague
RRDD, Reprocessing Group

Young Officer's Forum

Shri Arun Kumar Panda did his M.Sc in Physics from Hyderabad Central University in 2011. He joined Physical Metallurgy Division, IGCAR in the year 2012 after graduating from 55th batch of BARC training School. Presently, he is working as Scientific Officer-E. His research interests are studies of texture evolution in thin films, diagnostic of laser ablated plasma using Langmuir Probe and nano-indentation modeling by atomistic simulation.

Understanding the formation mechanism of SFT in FCC metals: An atomistic simulation study

Stacking fault tetrahedra (SFT)

SFT are three dimensional defects commonly observed in FCC metals and alloys. SFT are formed when such alloys are subjected to plastic deformation, irradiation by energetic particles and quenching from high temperature. The SFT are highly stable defects and act as an obstacle to dislocation glide during deformation causing work hardening, embrittlement and plastic instabilities. In case of irradiation, defects such as vacancies and interstitials are produced. Vacancies aggregate via diffusion forming clusters and voids. The void swells and material fails. The journey of voids initiated due to irradiation ultimately leads to form SFT. Hence, the study of SFT formation mechanism is very much important as they are detrimental to mechanical properties of materials.

1. SFT formation mechanism reported so far

There are two school of thoughts related to formation mechanism of SFT. One is involvement of Frank loop and the other is without the involvement of Frank loop. The reported literatures provide information on formation of SFT based upon Silcox-Hirsch mechanism with involvement of Frank loop, Stress assisted dislocation interaction without the involvement of Frank loop by Wang and thermal assisted diffusion via vacancy aggregation mechanism by Uberuaga. But, the formation of SFT with or without the Frank loop is still less clear. In this report, an attempt has been made to elucidate the plausibility of proposed mechanisms under

different conditions. Atomistic simulation has been carried out under optimized conditions to describe SFT formation taking into account a low Stacking fault Energy (SFE) Ag metal.

2. SFT formation via Silcox-Hirsch mechanism with involvement of Frank loop

To demonstrate the formation of SFT by Silcox-Hirsch mechanism in Ag, FCC system of 20x20x20 unit cells containing 32,000 atoms are created. The interaction between Ag-Ag atoms is described using embedded atom method potential developed by William. A triangular platelet containing 120 vacancies, 15 atoms on each edge, are removed in (111) plane. The average edge length of SFT with respect to 15 atoms is around 4.04 nm. Periodic boundary conditions are applied in all three directions and a time step of 1fs
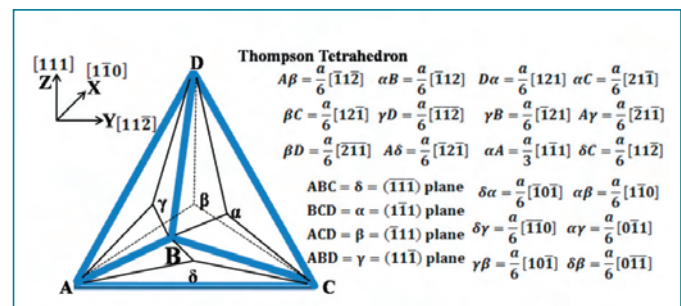
Figure 1: Schematic of a typical Thompson Tetrahedron describing slip systems ({111} planes) and dislocations of Shockley partials and Stair rods with their respective Burgers vectors of a/6 ⟨112⟩ and a/6⟨110⟩ in FCC crystals.
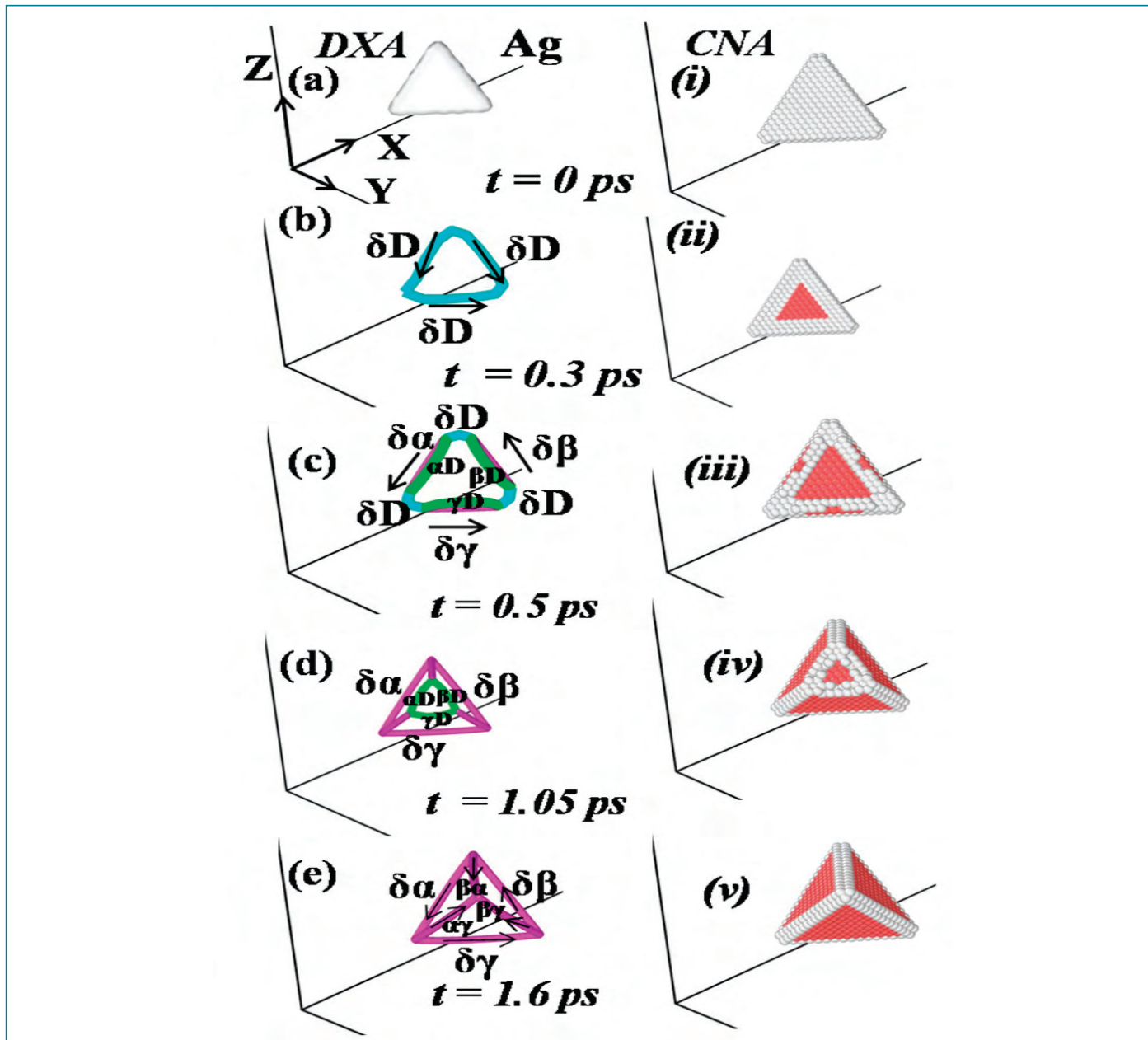
Figure 2: Atomic snapshots captured at different times by DXA (a-e) and CNA (i-v) methods to study the step wise evolution of SFT .The Shockley partial dislocation, Stair-rod dislocation and Frank partial dislocation are represented as green, magenta and cyan colours respectively by DXA method. Atoms in red and white colour are hexagonal close packed (HCP) atoms and other atoms in case of CNA method. Atoms in perfect FCC positions are removed for better view.

is chosen for the simulation. The entire energy of the system is minimized by conjugate gradient method to determine the minimum energy configuration. The static relaxation was achieved when the energy convergence criterion of 1.0e-10 is satisfied. The entire system was thermalised for 10000 molecular dynamic steps (10 ps) with time step of 1 fs using isothermal-isobaric (NPT) ensemble at a temperature of 1 K and pressure of 0 bar. Simulation results were visualized by Open Visualization Tool (OVITO) and the defect structures were analysed by adopting dislocation extraction algorithm (DXA) and common neighbour analysis (CNA) method.

The formation of SFT via Silcox-Hirsch mechanism is explained using Thompson Tetrahedron notation (See Figure 1) which is used to index the slip planes, Shockley partials and stair-rods with their Burgers. The tetrahedron is oriented in such a way that the Z-axis [111] is perpendicular to the plane ABC and coincides with δD. Figure 2 showed the atomic snapshots of step wise evolution and transformation of Frank loop to SFT. The triangular platelet of vacancies collapsed to a Frank loop (δD) with Burgers vector $\frac{a}{3}(\bar{1}\bar{1}1)$. As the triangular Frank loop was unstable, the three edges of the loop dissociated into stair-rod and Shockley partial dislocations.
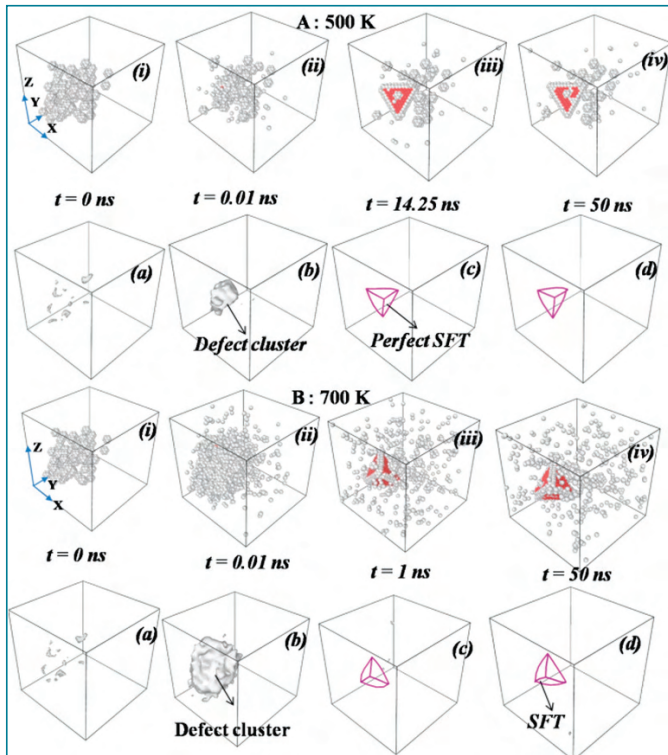
Figure 3 : Atomic snap shots on evolution of vacancies to produce SFT in case of Ag at temperatures of (A) 500 K and (B) 700 K. Both (a-d) and (i-iv) images show the atomic snapshots at selected time interval obtained from MD simulations using DXA and CNA methods.

These dislocation reactions are represented as:

δD→δγ+γD

δD→δβ+βD

δD→δα+αD
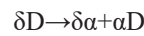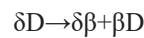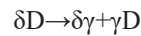
The leading partials γD, βD and αD glided on respective γ, β and α slip planes and met each other to produce stair rods of βα, αγ and βγ.

αD + Dγ→ αγ

βD + Dγ→ βγ

βD + Dα→ βα
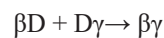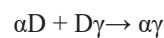
The edge part of leading Shockley partials move towards the apex of tetrahedra to produce a tetrahedron accompanying four Stacking faults on {111} planes and six stair rods (δγ,δβ,δα,αγ,βγ and βα) of Burger vectors $\frac{a}{6}\langle 110 \rangle$ along its edge. The Shockley partials during the formation of SFT are convex shaped due to the surface tension of stacking faults. At higher temperatures beyond 300 K, the stacking faults are degraded as local atoms
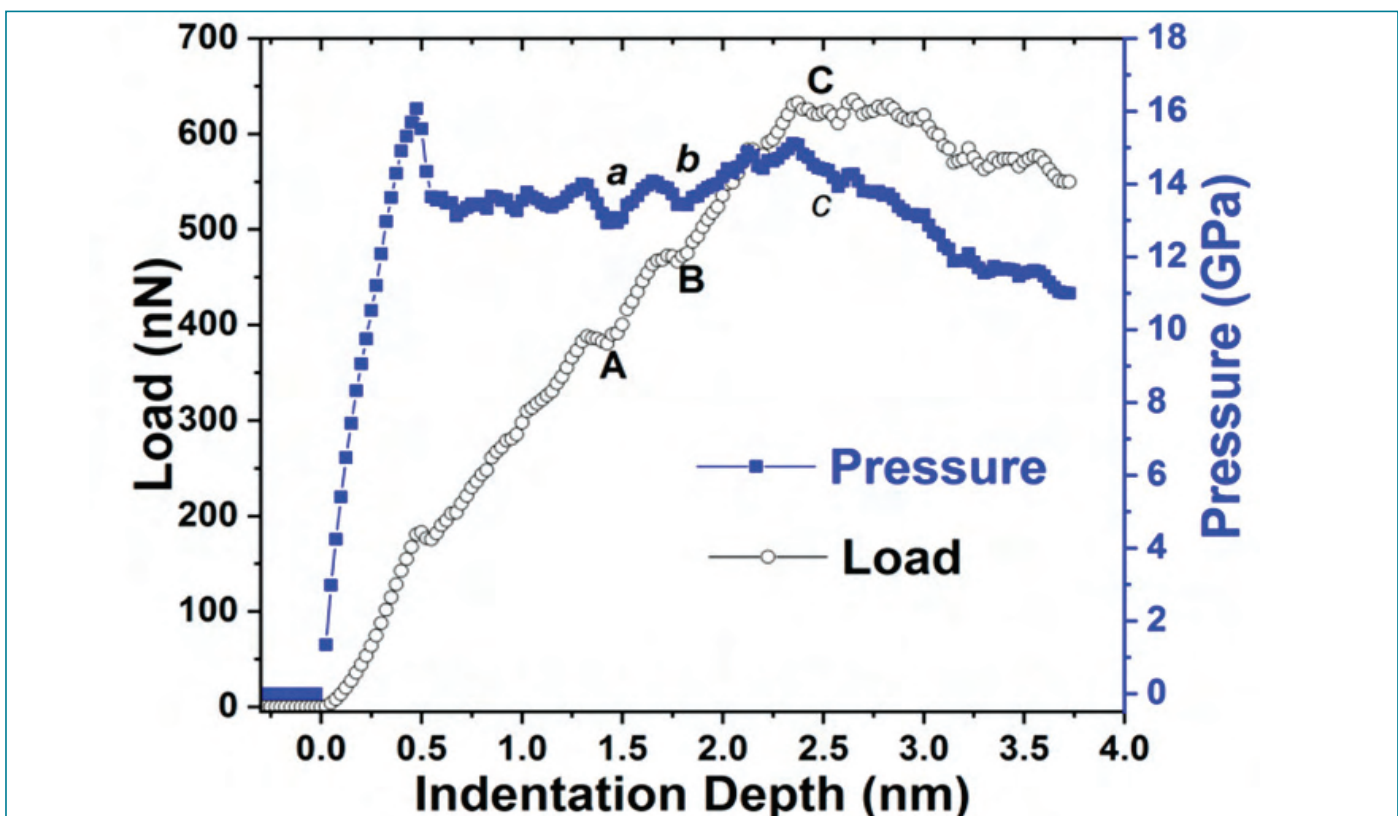
Figure 4: Load-Indentation depth and the corresponding pressure-indentation depth curves from MD simulations for [111] orientations of Ag at temperature of 1K.
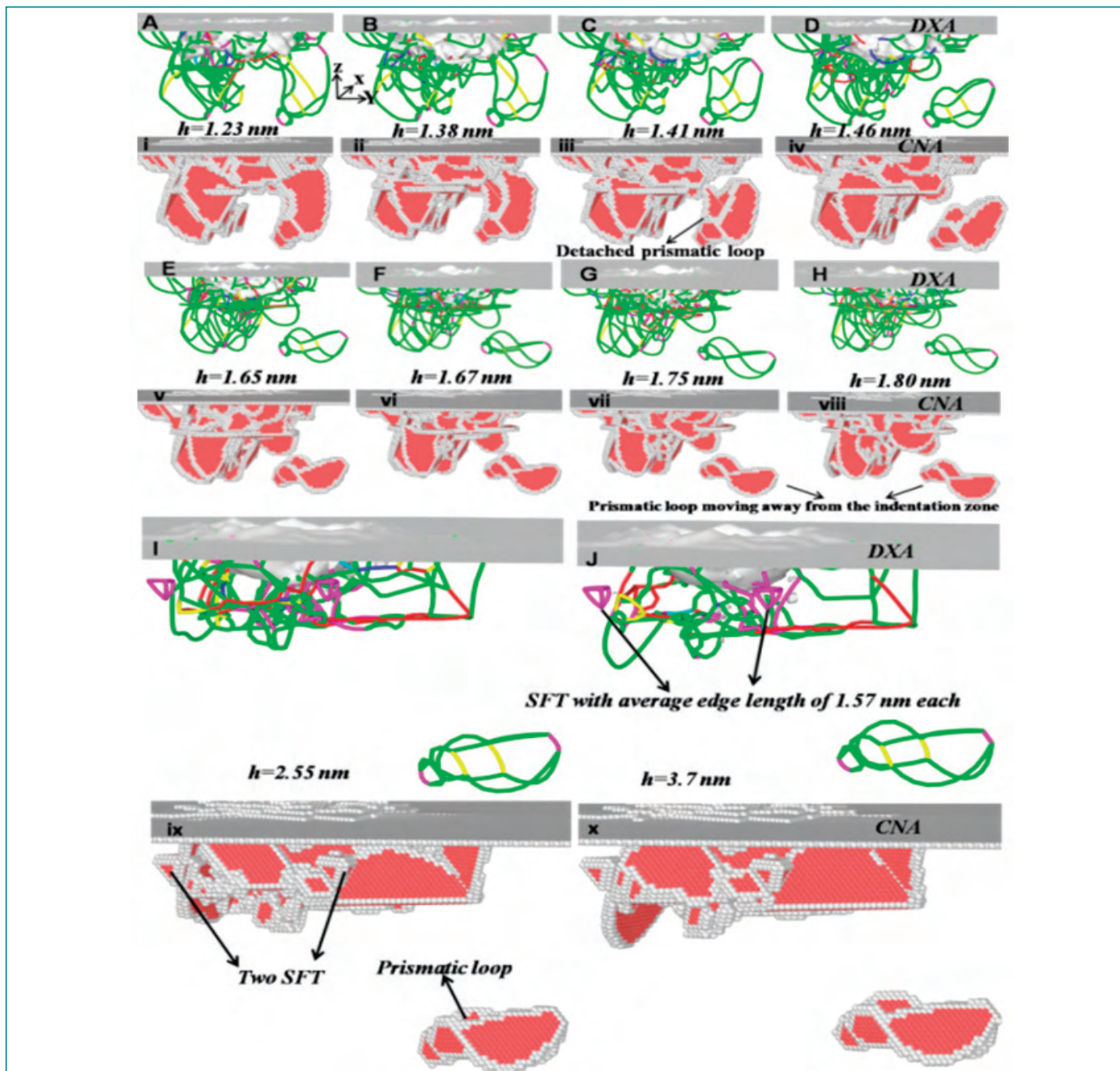
Figure 5: Visualisation of formation, movement of prismatic loops and SFT produced in Ag at different indentation depths using DXA and CNA methods.

become more disordered and perfect SFT are truncated. Hence, it is worth noting that Silcox -Hirsch mechanism is responsible for the formation of SFT during irradiation at low temperature.

3. SFT formation from random distribution of vacancies without involvement of Frank loop

To simulate SFT from random vacancies via diffusion-based vacancy aggregation mechanism, the systems are kept at prescribed temperature of 500 K, 700K for Ag using NPT ensemble and Nosé-Hoover thermostat throughout the simulation. The vacancies require

longer time to produce SFT at low temperature, because of lower rate of diffusion, whereas slightly higher temperature promotes the vacancy diffusion rate to form perfect SFT. With increase in further temperature, the atoms may become highly disordered affecting the stacking faults making the perfect SFT as truncated one. The chosen maximum temperature (700 K for Ag) are the homologous temperature ($\sim$0.5) of Ag which is determined from the reported melting point of Ag using Williams potential. Figure 3 (A) and (B) show the temporal evolution of free vacancies to produce SFTs during Molecular Dynamics (MD) simulation in case of Ag at
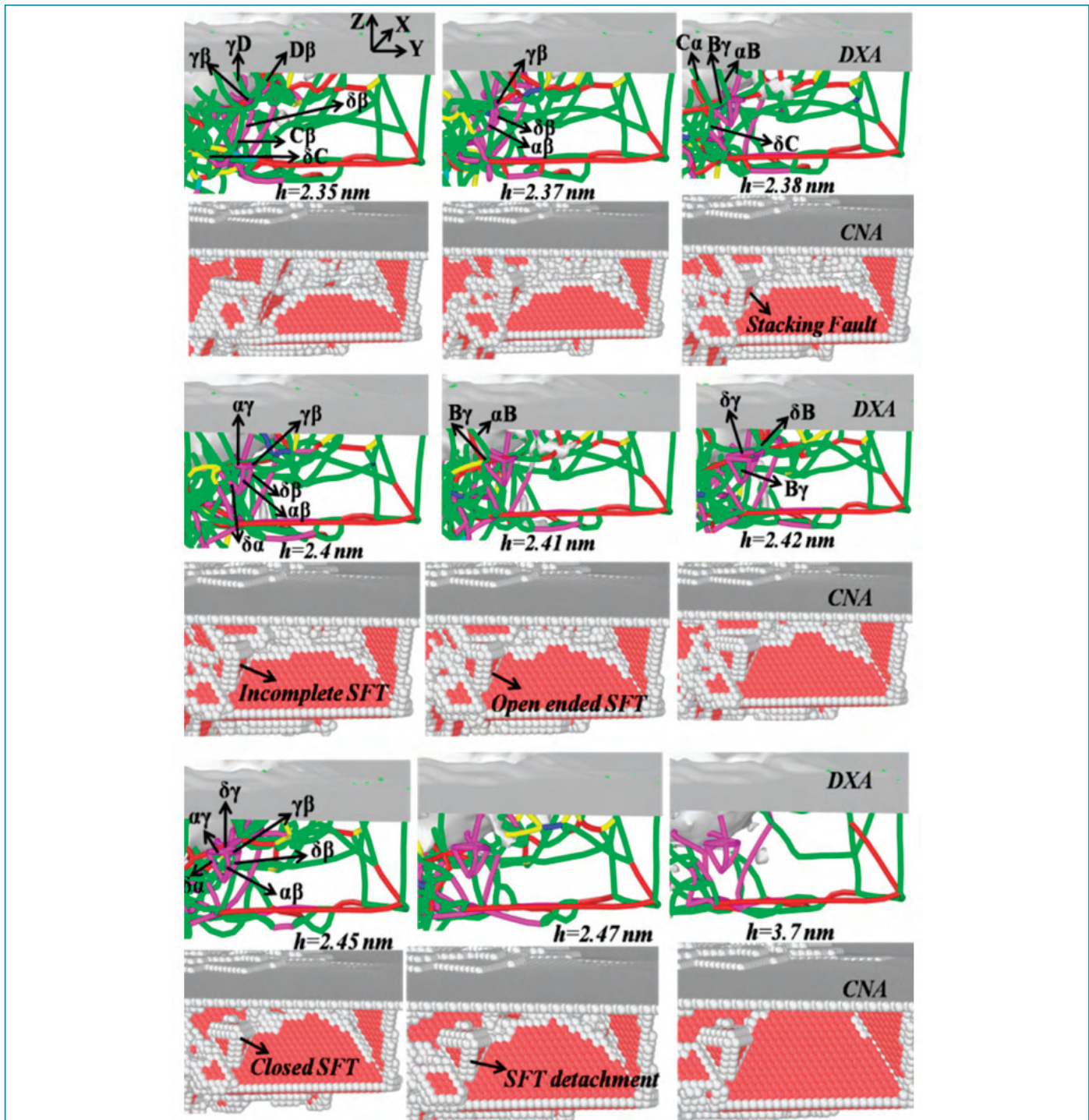
Figure 6: Step wise evolution of SFT formation during the process of indentation at different indentation depths in Ag. The detailed dislocation processes are derived using DXA and CNA methods.

different temperature of 500 K and 700 K respectively without the involvement of Frank loop.

Eighty-five vacancies are removed at random lattice site which are represented as white clusters using CNA method in Figure 3: A (i), B (i). The vacancies represent an individual entity at the beginning of simulation and started to cluster with time. The cluster collapsed to form a perfect SFT at temperature of 500 K containing 66

vacancies at 14.25 ns whereas at temperature of 700 K, the defect cluster evolved into one SFT at early stage of 1 ns consisting of 72 vacancies which is six less than the perfect stacking fault tetrahedron containing the magic number of 78 vacancies. The defect cluster collapsing to Frank loop was not stable at such high temperature and could not form SFT via Silcox-Hirsch mechanism. These simulations can be correlated experimentally

to the formation of single vacancies under irradiation at different temperature, forming clusters of any number of vacancy atoms or magic number of atoms. These clusters produced SFT by void collapsing without going through the Frank loop. As the Frank loop was not stable at higher temperature, the origin of SFT from free vacancies was less likely via Silcox-Hirsch mechanism.

4. SFT formation due to stress assisted dislocation interaction

To study the SFT formation due to plastic deformation, the load as a function of indentation depth is simulated for (111) surface of Ag using a spherical indenter of radius 4 nm. The Pressure ~ Indentation depth curve is plotted along with Load~Indentation depth in Figure 4 to comment on effect of pressure on dislocation loop and SFT. When the applied stress exceeded the critical resolved shear stress value, new sets of dislocation on different slip systems got activated to release the stress. The new sets of dislocations nucleated, splitted into partials and interacted to produce stable structure to relax the system. The Frank loop types of dislocation, though energetically favourable, were not observed very often underneath the indenter during indentation as compared to perfect dislocation (a/2 ⟨110⟩), Shockley Partials (a/6 ⟨112⟩), Hirth locks (a/3 ⟨100⟩) and stair rod dislocations (a/6 ⟨110⟩) which are represented as blue, green, yellow and magenta colours respectively in Figure 5. Hence, the effect of mechanical properties due to Frank loop was not significant. The dislocations introduced in the system during indentation underneath the indenter interacted to form SFT, which acted as strong obstacles to the motion of other dislocation contributing effectively to the plastic behaviour of materials. The post -yield (after transition from elastic to plastic region) Load~Indentation Depth and the corresponding Pressure-Indentation Depth curves exhibited series of drops in load and pressure. The drops (pop-in events) are marked by English alphabets in the curves. The drops (a,b,c,A,B,C) in load/pressure are due to bursting and detachment of dislocation loops/ SFT (See Figure 5) from the indent zone as a process of stress relaxation with decrease in hardness causing softening. Between two consecutive drops, there is rise in load/pressure with some fluctuations, indicating hardening as shown in Figure 4.

The step wise evolution of SFT because of dislocation interactions of Shockley partials are discussed below .To understand the step wise evolution of SFT in Ag, the particular regions of interest on formation of SFT at different indentation depths is shown in Figure 6. In this case, the formation of SFT is stress assisted as the effect of diffusion of atoms is ruled out at temperature of 1 K. It is evident that the entire atomistic process involved on formation of SFT in Ag is due to the interaction of partial dislocations and there is no involvement of vacancies or Frank loops. During plastic deformation under higher strain rate or indentation process, the dislocations are pumped into the system. The dislocation concentrations are higher compared to vacancy concentration; hence vacancy clustering to void or triangular platelet at temperature of 1 K is less probable. Therefore, dislocation interaction may be the only mode to form SFT during stress assisted process of nano-indentation. The role of Frank loop is less significant to produce SFT during plastic deformation. It is reported that Frank loop is only required to produce SFT under irradiation at low temperature , whereas vacancy clustering from single vacancies under irradiation at higher temperature (> 300 K) form SFT without the involvement of Frank loop in case of FCC metals.

This report highlights that Silcox-Hirsch mechanism with involvement of Frank loop is likely to form SFT during irradiation at low temperature whereas dislocation interactions without including Frank loop are probable to form SFT during plastic deformation.

Young Researcher's FORUM

Mrs. Vaddanam Venkata Sravani is working towards her doctoral degree from HBNI at the solution chemistry and mass spectrometry studies Section, MC&MFCG, IGCAR. She completed her bachelors degree in chemistry at Sri A.B.R Govt. degree college (Repalle-Andhra Pradesh) and masters in chemistry at Andhra university, Visakhapatnam. She is studying the post synthetic modification of metal organic frameworks for developing phosphors, and sensing/recovery of radionuclides. She has published five papers in peer-reviewed international journals so far towards her Ph.D Work. In addition, she has contributed to work published in another publication.

Post Synthetic Modification of Metal-Organic Frameworks for Development of Phosphors and Sensing / Recovery of U(VI)

Metal-organic frameworks (MOFs) are highly porous crystalline coordination polymers, exhibiting remarkable applications in various fields including gas adsorption/storage, catalysis, magnetism, drug delivery, membranes and sensing, owing to their properties such as high surface area, high porosity, tunable pore size, well ordered crystalline structure, magnetism and luminescence. Post Synthetic Modification (PSM) is the process of integrating various organic functional groups onto pristine MOFs to modify and change their physical and chemical properties without affecting the structural topology. PSM strategy also enables the synthesis of MOFs with enhanced structural stability. MOFs with amino pendants have harbored great attention for modification with desired organic functional groups by PSM strategies, offering different applications.

Designing luminescent phosphors tunable by light, have fetched significant attention among scientific community owing to their application in various scientific and technological areas such as chemosensors, light-emitting diodes (LEDs), biomedicine, etc. Rare earth free phosphors (REFP) are also suitable materials which garnered attention. It is important to look for rare earth free materials which are simple to synthesize, require less chemicals, easy to handle, tunable and environmentally benign.

Among all energy sources, nuclear power is a dense source of power which is environmentally benign. Uranium is the widely employed fuel in nuclear industry which is also highly toxic, environmentally. Uranium resources are limited and release of uranium into ecosystems is highly undesirable. Hence monitoring and regulating uranium is crucial. Therefore, it is important to
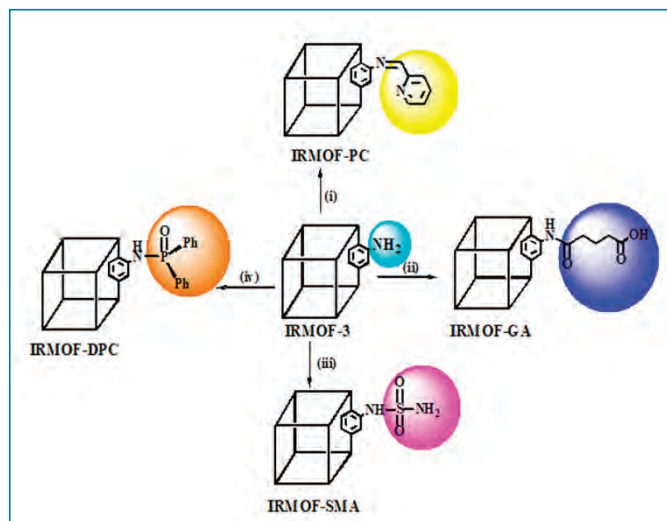
Scheme 1. PSM of IRMOF-3 with various functional groups: (i) 2-pyridine carboxaldehyde; (ii) glutaric anhydride; (iii) sulfamic acid;(iv) diphenyl phosphonic chloride.

develop materials for selective sensing of U(VI) and also for its recovery from aqueous medium.

In the last few years, iso-reticular metal organic framework-3 (IRMOF-3) has been widely used for various applications due to its high surface area (BET reports 2200 m^2/g), thermal stability ($\sim$400°C) and luminescence. The successful studies on PSM of amino-pendant MOFs and the properties exhibited by IRMOF-3, motivated us to perform studies on the photoluminescence, sensing and sorption of U(VI) from the aqueous medium using functionalized IRMOFs.
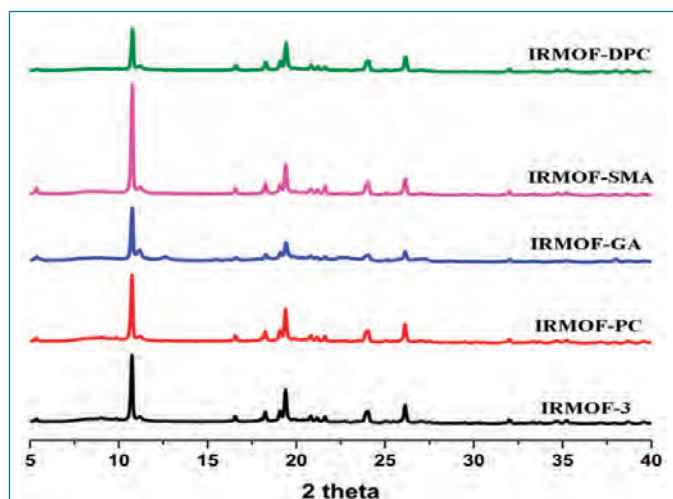
Figure 1: Powder XRD patterns of IRMOF-3 and its functionalized MOFs.

In this context, IRMOF-3 was synthesized by solvothermal method and PSM MOFs were prepared by incorporating different functional groups viz. 2-pyridine carboxaldehyde, glutaric anhydride, sulfamic acid, and diphenyl phosphonic chloride into IRMOF-3 (Scheme 1). The synthesized IRMOFs were characterized and employed for sensing and recovery of U(VI) from aqueous medium. In addition, IRMOF-3, IRMOF-SMA, and IRMOF-DPC were investigated for photoluminescence.

Different characterization techniques namely; FTIR, PXRD, TGA, NMR, SEM, and EDX were used to confirm the successful synthesis of functionalized IRMOFs. The IR spectra of PSM MOFs confirmed the presence of grafted functional groups. The PSM MOFs exhibit PXRD patterns similar to that of parent IRMOF-3 indicating the intact structure of IRMOF-3, with no apparent loss of crystallinity upon grafting of functional groups (Figure 1). NMR, SEM, and EDX also confirmed the formation of PSM MOFs.

U(VI) sorption studies from aqueous medium were carried out using IRMOF-3 and its PSM MOFs by batch method. For pH sorption studies, concentration of U(VI) (1000 mg/L), pH (2 to 9), contact time (180 min) were optimized at room temperature (25 ± 1 °C). About 10 mg of MOF was equilibrated with 3 mL of uranyl nitrate solution (1000 mg/L) for 3 h in an equilibration tube, at room temperature. Subsequently, the mixture was centrifuged for 10 min at 5000 rpm. The supernatant liquid was separated and used for the analysis of U(VI) by UV-spectrophotometry using Arsenazo-III as the chromogenic agent (λ_{max} = 655 nm). For kinetic studies, contact time was varied from 0 to 360 min following the same procedure mentioned for pH studies. The sorption efficiency (%), distribution coefficient (K_d), and amount of uranium adsorbed (q_e) onto MOFs were calculated using the following equations:

$$\text{Sorption efficiency (\%)} = \frac{C_0 - C_e}{C_0} \times 100 \quad (1)$$

$$K_d = \frac{C_0 - C_e}{C_e} \times \frac{V}{m} \quad (2)$$

$$q_e = \frac{C_0 - C_e}{m} \times V \quad (3)$$

Here, C_0 and C_e denote the initial and equilibrium concentrations (mg/L) of U(VI), V is the volume of solution (L), and m is the mass of sorbent (g).

U(VI) sensing studies were performed using IRMOF-3 and its PSM MOFs by making MOF suspensions (10 mg of MOFs in 25 mL of de-ionized water). Each test sample was prepared by mixing 250 μL of MOF suspension, varying concentrations of U(VI) solution (0 to 300 mg/L), 10 μL of 0.5 M NaNO$_3$, and remaining portion made up to 500 μL with ultra-pure water (pH 4). To investigate the selective sensing of U(VI) over lanthanides (La(III), Ce(IV), Nd(III), Sm(III), Gd(III), and Eu(III)) by IRMOF-3 and its PSM MOFs, fluorimetric sensing studies were carried out by considering 100 mg/L as standard concentration for all the metal ions.

The U(VI) sorption studies performed to understand the effect of pH revealed that the sorption of U(VI) strongly depends on pH (Figure 2). Sorption of U(VI) onto IRMOFs is low up to pH 4, which increases up to pH 6 for all MOFs and then decreases after pH 7. The modified IRMOF-DPC exhibits greater sorption behaviour (300 mg/g) than that of IRMOF-3 (239 mg/g). The increasing order of sorption capacity of U(VI) onto IRMOF-3 and PSM MOFs (Table 1) are as follows: IRMOF-3-DPC (300 mg/g) >IRMOF-SMA (292 mg/g) > IRMOF-PC (289 mg/g)>IRMOF-GA (280 mg/g) > IRMOF- 3 (273 mg/g). The improved sorption behaviour shown by IRMOF-DPC could be due to the strong electrostatic interaction between hard Lewis acid U(VI) and hard Lewis base: phosphoryl oxygen (P=O). The bonding efficiency of IRMOF-DPC towards U(VI) was further confirmed by IR spectroscopy. All the sorption parameters of U(VI) onto IRMOFs are presented in Table 1. In addition, desorption and recyclability studies have also been performed.

Table 1. Sorption of U(VI) onto IRMOF-3 and PSM MOFs (pH = 6)			
MOF	Sorption efficiency (%)	Kd	qe (mg/g)
IRMOF-3	91±2.73	3096±92.88	273±8.19
IRMOF-PC	96±2.88	8122±243.66	289±8.67
IRMOF-GA	93±2.79	4277±128.31	280±8.7
IRMOF-SMA	97±2.91	12384±371.52	292±8.76
IRMOF-DPC	99±2.97	24983±749.49	300±9.0
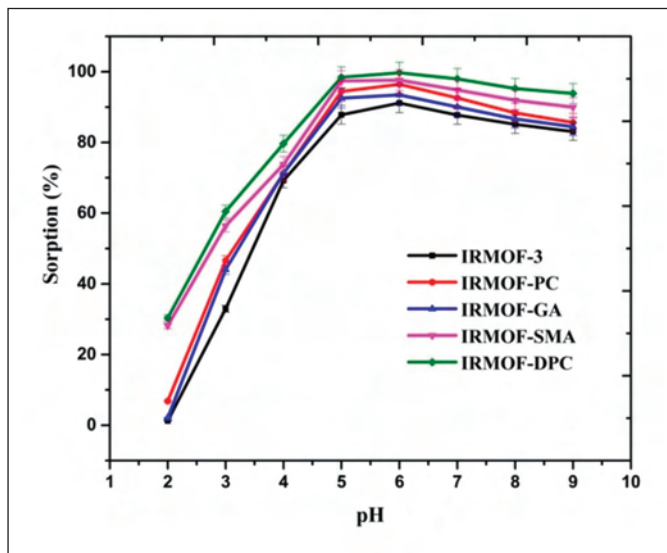
Figure 2: Effect of solution pH on U(VI) sorption efficiency (%) onto IRMOF-3 and its PSM MOFs, t =180 min, msorbent= 10.0 mg, Vsolution=3 mL, Co= 1000 mg/L, T=25 ±1^{0}C.

Figure 4. Quenching (%) of IRMOF-GA with U(VI) and competing metal ions (100 mg/L) (La(III), Ce(IV), Nd(III), Sm(III), Gd(III), and Eu(III).

IRMOF-3 and its PSM MOFs were examined for fluorescence sensing of uranyl ions. All the MOFs except IRMOF-DPC show good quenching when concentration of U(VI) is 6.25 mg/L. The quenching of fluorescence intensity of the MOFs at 6.25 mg/L of U(VI) shows the following trend: IRMOF-SMA (65.4%) > IRMOF-3 (64.3%) > IRMOF-PC (63.5%) > IRMOF-GA (58.6%) > IRMOF-DPC (10.9%). Out of five IRMOFs, IRMOF-GA is most sensitive to U(VI) (Figure 3a). Even 1 mg/L of U(VI) quenches the fluorescence intensity of the MOF by nearly 30%. The detection limit (3σ/slope) was calculated to be 0.36 mg/L, clearly demonstrating the potential application of IRMOF-GA as quantitative sensor for U(VI). Langmuir model was used to fit the fluorescence quenching ratio [((I0-I)/I0) x100] and the graph was plotted between quenching ratios vs U(VI) concentration. On transforming the simulated Langmuir equation

to a relation between U(VI) concentration (C) and C/[(I0-I)/I0x100] (Figure 3b inset), a near linear correlation was obtained.

In order to investigate the selective sensing of U(VI) over other metal ions from aqueous medium using IRMOF-3 and its PSM MOFs, lanthanide ions (La(III), Ce(IV), Nd(III), Sm(III), Gd(III), and Eu(III)) were chosen for fluorescence studies. The quenching of fluorescence intensity of all MOFs by lanthanides was found to be in the range of 2 to 53% for 100 mg/L of lanthanides (Figure 4). However, it is to be noted that this quenching is lower than that for the same amount of U(VI) (~98%) indicating that all MOFs were highly selective for sensing of uranyl ions.

IRMOF-3, IRMOF-SMA and IRMOF-DPC were also investigated for color tunable phosphor studies. To understand the luminescence
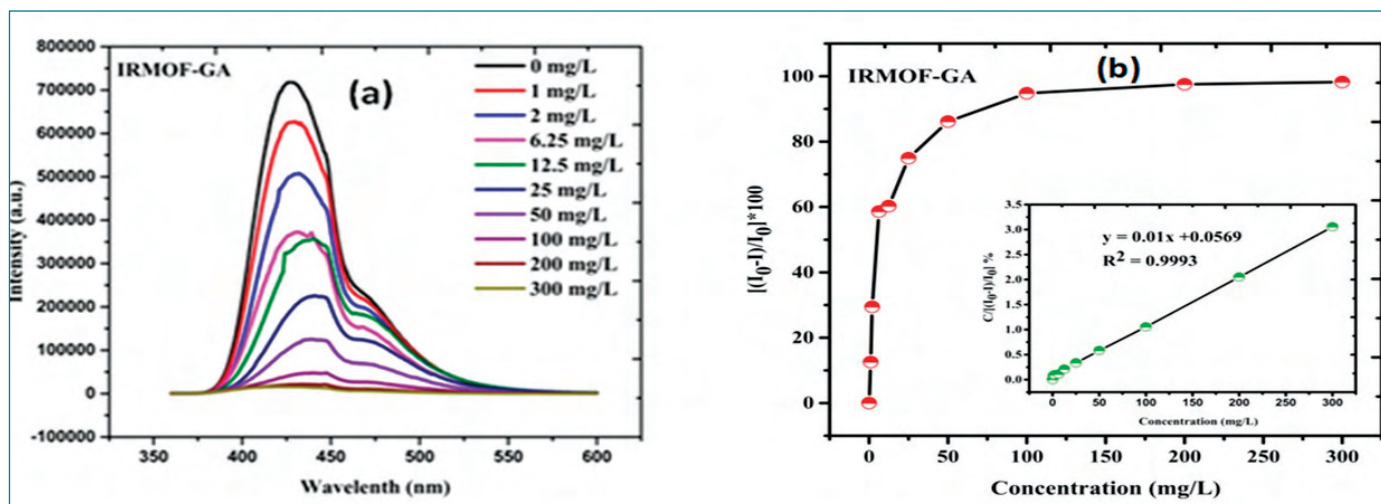
Figure 3. (a) Emission plot of IRMOF-GA with respect to U(VI) concentration; (b)The effect of U(VI) concentration on quenching (%) of IRMOF-GA.
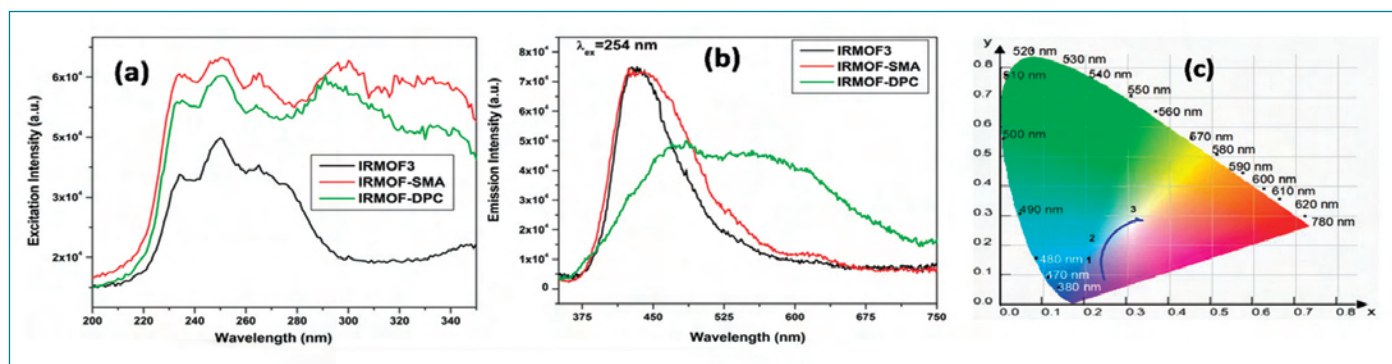
Figure 5 : (a) PL excitation (b) PL Emission and (c) Color Coordinate diagram of IRMOF-3, IRMOF-SMA, and IRMOF-DPC.

intensity of IRMOFs, PL excitation and PL emission spectra were recorded. Figure 5a shows the PL excitation spectra of IRMOF-3, IRMOF-SMA and IRMOF-DPC. The pristine IRMOF-3 sample displayed a broad band colored in the region 220-280 and excitation spectra of IRMOF-SMA, IRMOF-DPC have similar feature till 280 nm with evolution of additional bands at 290 and 330 nm. It seems all these three bands have similar origin. Figure 5b shows the emission spectra of pristine and PSM MOFs under 254 nm excitation. The emission spectra of IRMOF-3 displayed a narrow emission peak with maxima around 425 nm in violet region with FWHM ~80 nm. On the other hand, IRMOF-SMA displayed emission peak at 454 nm with FWHM~100 nm. Furthermore, IRMOF-DPC displayed very broad bands consisting of dual features at 470 and 570 nm. To identify the actual color of light emitted by IRMOF samples, color coordinate values using corrected emission spectra were also calculated (Figure 5c).

The color coordinate values clearly reflect violet, blue and near white light emission respectively from IRMOF-3, IRMOF-SMA, and IRMOF-DPC. The correlated color temperature (CCT) is a very important parameter for near white light emission in order to predict its actual color hue. In the case of IRMOF-DPC under 254 nm excitation, CCT value was found to be 5773 and hence the white light emitted by IRMOF-DPC under 254 nm π-π^* excitation is cool white in nature.

The luminescence decay profile for both pristine and PSM IRMOFs depicted biexponential profile. The decay curve could be fitted using equation 4.

$$I = I_0 + A_{1exp} (-t/\tau_1) + A_{2exp} (-t/\tau_1) \qquad (4)$$

Here, I_0 is background or zero offset, A_1 and A_2 are the intensities at different time intervals and τ_1 and τ_2 are their corresponding lifetimes. The average lifetime values clearly confirmed the enhancement in average luminescence from 5.87 μs for pristine to 6.93 μs for IRMOF-SMA and 12.9-15.7 μs for IRMOF-DPC (Table 2).

Table 2: Luminescence lifetime values for IRMOF-3, IRMOF-SMA and IRMOF-DPC

MOF	τ_1 (μs)	τ_2(μs)	τ_{avg} (μs)
IRMOF-3	2.43 (25 %)	1.88 (75 %)	5.87
IRMOF-SMA	3.28 (25 %)	13.88 (75 %)	6.93
IRMOF-DPC (λem=470)	13.54 (84 %)	157.76 (16 %)	12.90

In the present study, four PSM MOFs namely, IRMOF-PC, IRMOF-GA, IRMOF-SMA, and IRMOF-DPC were synthesized via PSM strategy using IRMOF-3. Synthesized MOFs were thoroughly characterized and studied for the sensing and recovery of U(VI) from aqueous medium. All the MOFs exhibit excellent sorption capacity towards U(VI) (>90%) and maximum uptake was observed by IRMOF –DPC (300 mg/g) at pH 6. IRMOF-GA offered impressive detection limit (0.36 mg/L). Moreover, these MOFs furnished excellent selectivity via fluorescence quenching for U(VI) (~98%) over other lanthanide ions (La(III), Ce(IV), Nd(III), Sm(III), Gd(III), and Eu(III)) (2-53%). The luminescence studies confirmed the huge color shift from violet (IRMOF-3) to bluish white region (IRMOF-DPC), upon PSM. Luminescence lifetime measurements suggested the linear enhancement in average lifetime from pristine (~5.9 μs) to IRMOF-SMA (6.9 μs) and IRMOF-DPC (~15.7μs). This strategy is useful for studies towards the synthesis of solid-state sorbents for sensing and efficient recovery of U(VI) from aqueous media and could also open up new avenues for future research in the field of developing rare earth free phosphors by tunable luminescence on MOFs via PSM strategy.

Azadi ka Amrit Mahotsav
Indira Gandhi Centre for Atomic Research
Program on Anu Awareness – a brief report

July 23 – August 12, 2022
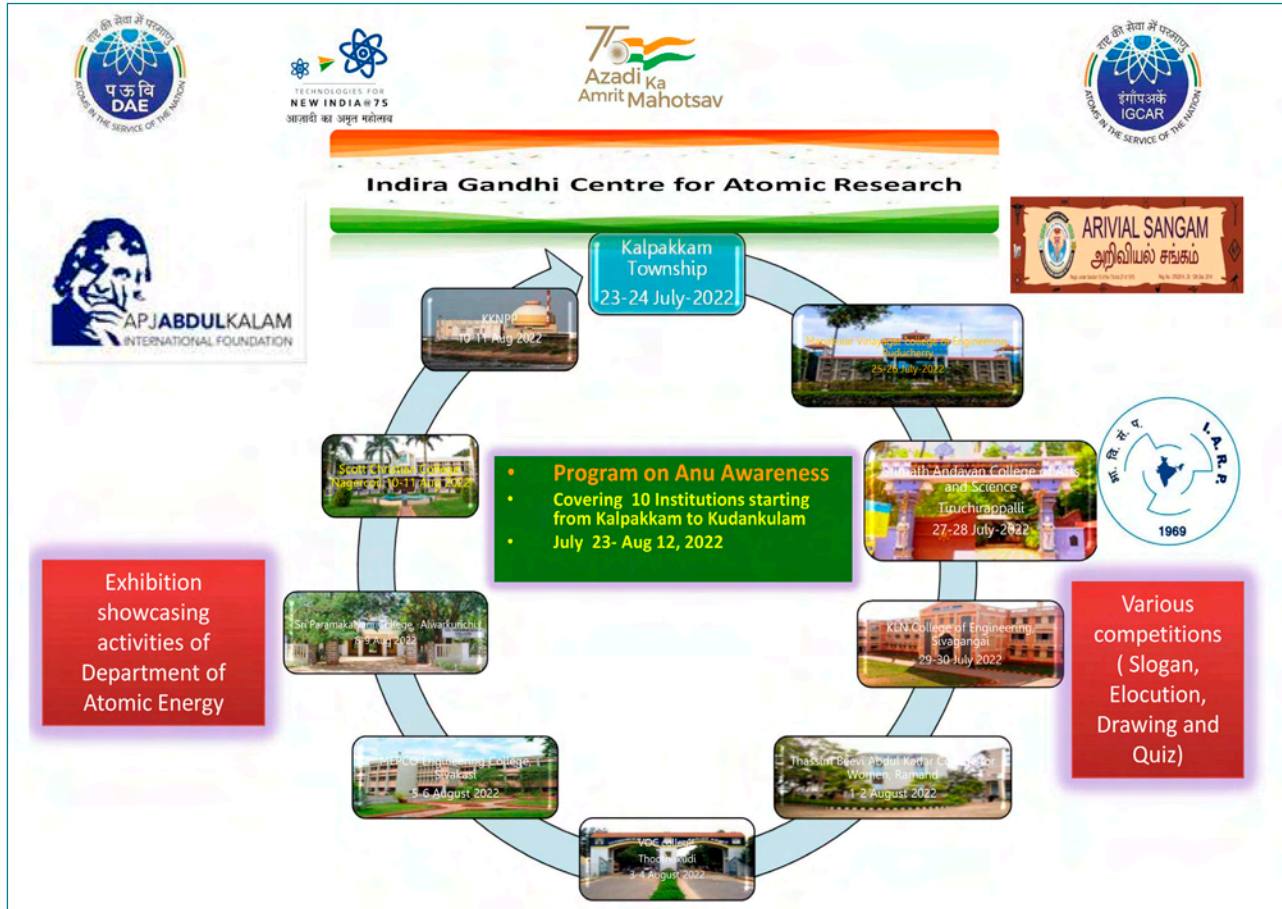
Figure 1: The nodal college venues

As a part of Azadi ka Amrit Mahotsav celebration, IGCAR has organised a sequence of awareness program to showcase and celebrate the technology development carried out and transfer of certain technology in the application of societal benefits by Department of Atomic Energy for the past 75 years after independence. The program is organised in association with A. P. J. Abdul Kalam International Foundation, Rameswaram, The Tamil Nadu Ariviyal Sangam and Indian Association for Radiation Protection. The program is started with curtain raiser event at Kalpakkam on 23-July-2022 and culminated at Kudankulam on 12-Aug-2022 covering 1100 kms in 10 nodal institutions. The sequential venues (colleges) along with event dates and the route map of the program is given in Figure 1 and Figure 2, respectively.

The program is a two days event in each nodal institutions comprising of various competitions and exhibition. The nodal institutions were asked to coordinate with schools and colleges in their educational division to participate in the program.

Figure 2: The route map of Anu Awareness Program

The nodal institutions are identified with the help of Tamil Nadu Ariviyal Sangam. The program is organised in each institutions by inviting a nodal personality as a chief guest of their choice and AD/GD level officials of IGCAR along with a crew of officers for the conduction of events and interactions.

Table 1: The details of each event viz. venue, officers from IGCAR, Chief guests and foot falls.						
Dates	Place	Institution	SQRMG Officers: Dr/Shri/Ms	Chief Guest (GDs)/Top officials*	Guest of Honors	Foot fall
23-24, July 2022	Kalpakkam	KV-1,2 and AECS-1,2,3 HSS, Pudupatinum and Sadras Kalpakkam	V. Subramanian and S. Chandresekaran	Director, IGCAR. CS, MAPS, Facility Director, INRPK Director, GSO CAO, IGCAR CAO, GSO	Shri A.P.J Salim Founder Dr.A.P.J Abdul Kalam Internation Trust Shri Gopal Parthasarathy, Secretary Tamil Nadu Ariviyal Sangam	1300 students
25-26, July 2022	Puducherry	Sri Manakkula Vinayagar Eng College, Pondicherry	Jalaja Madhanmohan, Vijaya Gopal, Krishnan Hemnath Dr. Kannan Ramu	Dr. B. K. Nashine Director, ESG and GSO	Shri Arun Nagalingam, VIBHA, Tamil Nadu Ariviyal Sangam	2500 students
27-28, July 2022	Tiruchirappalli	Srimad Andavan College, Tiruchirappalli.	Dr. Ponraju Mathiarasu Jalaja Madhanmohan, Hemnath Dr. Ganesan Ramu	Dr. Ponraju AD, HSEG, SQRMG	Dr. Mani Pragspathy, Joint Secretary, VIBHA	1800 students
29-30, July 2022	Sivagangai (Madurai)	K L N Eng Collge Pottapalayam, Sivagangai.	Dr. Ponraju Mathiarasu Jalaja Madhanmohan, Hemnath Dr. Ganesan Ramu	Dr. Ponraju AD, HSEG, SQRMG	Dr. Jeyakanthan State Trustee, Tamil Nadu Ariviyal Sangam	2000 students
01-02, Aug 2022	Ramanatha puram	Thassim Beevi Abdul Kader College for Women Ramanathapuram	O. Annalakshmi Madurai Meenachi Dr. Prabhakaran Parthipan Dr. Kannan	Dr. S. Ananthasivan Director, RpG	Madam. APJM Mazima Marakkayar, Trustee, A. P. J Abdul Kalam International Foundation	1500 students
03-04, Aug 2022	Tuticorin	V O Chidamabaram College Thoothukudi	O. Annalakshmi Madurai Meenachi Dr. Prabhakaran Parthipan	Shri T. K. Ramachandiran, IAS, CEO, VOC Port Trust, Tuiticorin	Shri Gopal Parthasarathy – Participated with teachers	2000 students
05-06, Aug 2022	Sivakasi	MEPCO Schlenk Eng. College, Sivakasi	M. Manohari R. Ramar Dr. Prabhakaran Parthipan	Shri S. Athmalingam Former , Associate Director RESG, SQRMG	Dr. Mani Pragspathy, Joint Secretary, VIBHA	3500+ students
08-09, Aug 2022	Alwarkuruchi	Sri Paramakalyani College, Alwarkuruchi	CAO, IGCAR EO, GSO Jalaja Madhanmohan Parthipan Ramu	Shri S. A. Murugasan, IAS, IFA	Dr. V. Parthasarathy, Vice President, Tamil Nadu Ariviyal Sangam	1800 students including about 80 Students from Hearing and speech impaired.
10-11, Aug 2022	Nagercoil	Scott Christian college Nagercoil]	Chandrasekar Bramha Jalaja Madhanmohan Ramu	Dr. James R Daniel General secretary, Kanyakumari Academy of Science & Arts		3000 students
12 Aug 2022	KKNPP Kudankulam	Community hall, kknpp township	Dr. V. Subramanian Chandrasekar Bramha Jalaja Madhanmohan Ramu	Director IGCAR, SD, KKNP 1&2, CEE, KKNP 5&6	Shri A. P. J. Salim Founder Dr. A. P. J Abdul Kalam Internation Trust Dr. Umaiorubhagan, President, Tamil Nadu State Ariviyal Sangam	500 students

About the event: Each event is highlighted with foot fall of about 2000 students. The detailed list of institutions, their places, chief guests of the respective events, number of foot falls for the events are given in Table 1. The competitions include, Elocution, Slogan writing, Drawing and Quiz. The competitions are held in two categories viz. up to school level students and college students comprising of about 250 students in each category. The general topic for all the competitions is "Science Development in India for the past 75 years after independence". The exhibits cover the working models of three stage reactors, Bhabhatron and Gamma Irradiation Chamber along with panels on DAE technologies to the application of societal benefits. In addition to the above, a tree plantation event of about 100 saplings is organised in each institutions towards environmental care. The tree plantation event is organised in association with APJ Abdul Kalam International Trust.

Reported by
V. Subramanian, SQRMG

DAE-ICONIC Week Celebration
Indira Gandhi Centre for Atomic Research
August 22-28, 2022

SAND ART Sculpture

As a part of Azadi ka Amrit Mahotsov (AKAM) -DAE ICONIC week Celebrations, IGCAR and GSO, have organised a sand art sculpture in the Kalpakkam beach during Aug 27-28,2022 depicting various technologies of DAE applied to the societal benefits, highlighting contribution to power sector, agriculture, health and technology development . The sculpture was inaugurated by RDO, Chengalpattu Smt. Shajeevana, IAS, in the presence of President of Pudupattinam Panchayat, Senior Commandant, CISF and officials of IGCAR & GSO, Principals and students of AECS and KVs. Flood light arrangements were made. Wide publicity

Inauguration of Sand Art Sculpture at Kalpakkam Beach by Tmt. R. V. Shajeevana, IAS, RDO, Chengalpattu along with Dr. B. Venkatraman, Distinguished Scientist, Director, IGCAR

was given. There were more than 20000 foot falls from the residents of DAE Townships, Pudupattinam and Sadurangapatinum villages.

Reported by
V. Subramanian, SQRMG

DAE-ICONIC Week Celebration
Indira Gandhi Centre for Atomic Research
August 22-28, 2022

Generation of Magic Square - 750 Squares using 75 iconic dates of DAE with 75 Students

As a part of Azadi ka Amrit Mahotsov and DAE ICONIC week Celebrations during August 22-28, 2022, IGCAR has organised an one day event on 22-08-2022, in the Higher Sec School, Sadurangapattinam. The event was planned as "Generation of Magic Squares" of 750 squares with 75 students from nearby Higher Secondary Schools (State board) of Kalpakkam in the Chenglepet Educational District, to commemorate 75 years of Independence using 75 numbers of important milestone dates of Department of Atomic Energy. The program was conducted by a mathematician Shri Jothi Lingam, Retd., Station Master, Indian Railway.

The details of the school:

The School	Number of Students
Govt Higher Sec School, Sadurangapattinam	12
Govt Higher Sec School, Pudupattinam	09
Govt Higher Sec School, Vayalur	09
Govt Higher Sec School for Girls, Thirukkazukundarm	09
Govt Higher Sec School, for Boys, Thirukkazukundram	09
Govt Higher Sec School, Vengambakkam	09
Adi Dravidar Welfare Govt Higher Sec School, Manamai	09
Govt Higher Sec School, Mamallapuram	09

Figure 1: Generation of magic square

The program started with Tamil Thai Vazthu by school students of Sadurangapattinam followed by lighting of lamp. The program was inaugurated with a self composed Tamil Song about Atoms in the service of Nation sung by Nursery School Children of Pavalaru Tamil School, Kalpakkam. The welcome address was given by Head Mistress, Sadurangapattinam. The program was presided by President, Panchayat Board, Sadurangapattinam. The chief guest of the program was Dr. B. Venkatraman, Director, IGCAR.

The generation of magic square was carried out with iconic dates of DAE. A booklet on the compilation of 750 magic square has been prepared. The sample work sheet is shown in Figure 1. The participation certificate is issued to all the students and mementoes for the teachers.

Reported by
V. Subramanian, SQRMG

DAE-ICONIC Week Celebration
Indira Gandhi Centre for Atomic Research
August 22-28, 2022

Anu Walkathon - 2 km stretch using 100 iconic dates of DAE with 150 Students

As part of the Azadi Ka Amrit Mahotsav and DAE Iconic Week Celebrations, a series of programmes were organised by IGCAR, Kalpakkam during 22-08-2022 to 28-08-2022.

Anu Walkathon was organized on August 28 2022 by IGCAR at Elliot's beach Chennai. Dr. B. Venkaraman, Director, IGCAR welcomed the gathering and Shri S. Raghupathy, Director, RD&TG and Director, EIG briefed the participants about DAE and its activities. The walkathon was flagged off by Shri R. K. Kaushal Special Director General, CPWD and Dr. G. A. Ramadass, Director NIOT from Rajaji Bhavan, Besant Nagar. The Anu Walkathon team proceeded to the Elliot's beach, Besant Nagar with necessary Police support covering a 2 km stretch. 150 students from various city colleges and 100 public including DAE employees both serving and retired, participated in the walk for nuclear energy - Atoms in the Service of Nation. The participants were addressed by all senior officers from CPWD, NIOT, Madras University, Ariviyal Sangam and IGCAR. The walkathon concluded by returning back to Rajaji Bhavan. All police personnel, NSS coordinators and the eminent guests from other departments were facilitated. The student participants pledged their

Senior officers from CPWD, NIOT, Madras University, Ariviyal Sangam and IGCAR.

support for Nuclear Energy and there was a much appreciation by all the participants for such an event. IGCAR acknowledge the support of Ministry of Youth Affairs & Sports, CPWD and Tamilnadu Police department for the success of the event.

Reported by
V. Subramanian, SQRMG

HBNI-IGCAR CI

Ph.D Thesis Defense

Name	Title	Discipline
Telagathoti Suresh Kumar	Thermo Mechanical Fatique Evaluation of 316LN Austenitic Stainless Steel Welds and Weld Joints	Engineering Science
C. Praveen	Influence of Nitrogen on Tensile and Creep Deformation Behaviour of Type 316L Stainless Steel in the Framework of Internal - State - Variable Approach.	Engineering Science
Bommadeni Arun	Optimization of sampling and measurement techniques for Tritium and Carbon-14 in the atmosphere.	Chemical Sciences
L. Shirley Auxilia	Synthesis, characterization and leaching studies of $Ca_{10}(PO_4)_6X_2$, (X= OH, F) and its simulated radionuclide (Re, Cs, Nd, Sr) substituted analogues for the immobilization of radioactive waste	Chemical Sciences
M. Raghu Ramaiah	Photoinduced Deflection Studies in Si Micro cantilevers: Role of Incident Laser Parameters and Micro cantilever Dimensions.	Physical Sciences
Pew Basu	Studies on shielding effectiveness of composite materials and build-up factors for stratified configurations	Physical Sciences
R. Rajitha	Study of the phase transformations in some insensitive secondary explosives using Raman spectroscopy, XRD and DFT calculations	Physical Sciences

Certificate of Appreciation

Name	Title	Discipline
Mr. Choudhury Abinash Bhuiyan	Growth of Electronic Grade Monolayer MOS_2 using Chemical Vapour Deposition	Chemical Sciences

Awards, Honours and Recognitions

Dr. John Philip and Dr. Vasudevan featured in the world's top 2% Scientist list in the career-long category with 128,190, and 255,412 ranks, respectively published by Elsevier and Standford university in 2022.

Dr. John Philip, Dr. Vasudevan and Dr. B. B. Lahiri featured in the world's top 2% Scientist list in the single-year category with 46,826, 100,534 and 215,992 ranks, respectively published by Elsevier and Standford university in 2022.

Manali Nandi, SMARTS, MCG received the Best PhD Research Award (Physics) 2022 of Dr. K. V. Rao Scientific Society, Hyderabad for the thesis "Inter-droplet force measurement between gamma alumina Stabilized Pickering nanoemulsion droplets: role of electrostatic and electric dipolar interactions"

Dr. Geetisubhra Jena, CSTD, MCG, received the Best thesis award by NACE International India Section – during CORCON 2022, 19th – 22nd September, Udaipur, India for her thesis titled "Development of graphene oxide based composite coating with improved corrosion resistance and antibacterial properties".

E. Premkumar, SIRD, IGCAR won the Bronze medal on Uganda Para-badminton International tournament 2022 in both Men's Singles and Men's Doubles categories.

Best Paper Award

Reshma. T. S, Sourav Pan and Arindam Das
Selective Adsorption and Fast Photocatalytic Degradation of Mixture of dyes by Uncapped SnO2 QDs.
International Conference on Frontiers for Technological Applications (FIMTA 2022) (Gold Medal)

Dr. Anandkumar, Surdharshan, T. Nandakumar, Ravishankar and J. Philip of CSTD received the Best Poster Award of CORCON 2022 held during Sept 19-22, 2022 for the poster titled "Development of silane-based epoxy hybrid coating on water transporting pipeline materials for enhanced microbiologically influenced corrosion protection performance"

Bio-diversity @ DAE Campus, Kalpakkam

© SIRD, IGCAR
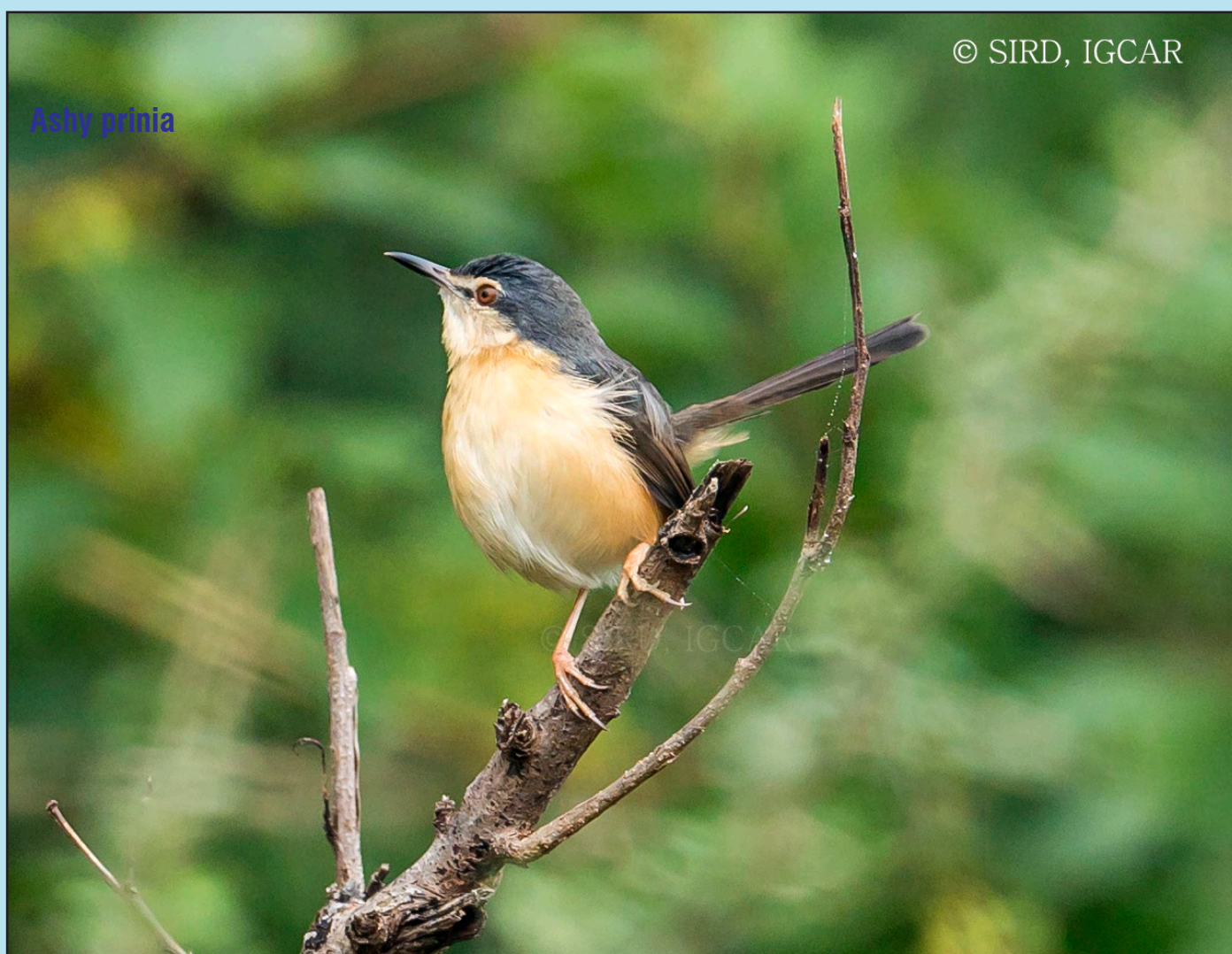
Ashy prinia

Ashy prinia was formerly known as ashy wren-warbler. It is a small bird with ashy grey upperparts and white under parts. They have a long graduated black and white tipped tail and it bobs up and down frequently. Both male and female are similar in size and appearance.